The role of the constitutive model in creep crack growth modelling

Abubakker Sithickbasha A[a], Sivasambu Mahesh[a,*]

[a]*Department of Aerospace Engineering, Indian Institute of Technology Madras, Chennai 600036 India.*

Abstract

Although high-temperature material response is known to be history-dependent, many models of creep crack growth assume the history-independent Norton constitutive law. Even so, these models capture the experimentally observed creep crack growth by adjusting only the damage model. This is explained presently by showing that the damage evolution ahead of a stationary crack in a material obeying a history-dependent unified creep-plasticity constitutive law due to Robinson can be 'fit' by simply adjusting the damage parameters in a model implementing Norton's law. The implication of this result to the case of propagating cracks is discussed.

Keywords: creep crack growth, constitutive law, stainless steel, continuum damage

1. Introduction

Crack growth in a creeping body has been the subject of a large number of theoretical, computational and experimental studies extending at least over the past five decades [1]. A number of models of creep crack growth, based on the local approach, have been proposed to predict the creep crack growth history in standard test specimen [2, 3, 4, 5, 6, 7, 8, 9, 10, 11, 12]. Many of these models successfully capture the experimentally observed creep crack growth rate in many high temperature materials including austenitic stainless steels.

Creep crack growth models based on the local approach are based on finite element analysis and continuum damage mechanics. The finite element analysis accurately predicts the spatiotemporal variation of all mechanical and damage fields for arbitrary inputs of inelastic constitutive law, and damage evolution law. The constitutive law typically accounts also for the current local damage. The exceedance of a threshold by the damage variable at select points in the

*Corresponding author

Email addresses: `ae13m001@smail.iitm.ac.in` (Abubakker Sithickbasha A), `smahesh@iitm.ac.in` (Sivasambu Mahesh)

domain is taken to indicate local material failure. In creep crack growth simulations, local material failure typically occurs ahead of the pre-existing crack, and signifies crack propagation. Algorithmic schemes such as setting the local stiffness to zero [4, 11, 12] or releasing displacement continuity constraints on nodes [4, 5, 10] are employed to represent crack propagation within the finite element analysis. Progressively more sophisticated damage evolution laws are due to Nikbin et al. [3], Saanouni and Chaboche [4], Yatomi et al. [5, 6, 8], Oh et al. [10] and Wen et al. [11, 12].

The creep constitutive law in all aforementioned models is independent of the loading history, i.e., the strain-rate depends only on the instantaneous state of stress and damage. Commonly, the assumed constitutive law is a variant of

$$\dot{\boldsymbol{\epsilon}}_{\mathrm{cr}} = \frac{3}{2}\left|\frac{\sigma_{\mathrm{eq}}}{\sigma_0(1-\omega)}\right|^n \frac{\boldsymbol{\sigma}'}{\sigma_{\mathrm{eq}}}. \tag{1}$$

Here, $\dot{\boldsymbol{\epsilon}}_{\mathrm{cr}}$ denotes the creep strain-rate, $\boldsymbol{\sigma}'$ denotes the deviatoric stress, σ_{eq} denotes the scalar equivalent stress, and σ_0 denotes a reference stress. ω, $0 \leq \omega \leq 1$ denotes the damage variable, and n is called the Norton exponent. Eq. (1) demonstrates also the involvement of the damage variable in the constitutive response.

The creep constitutive response is well-known to be history dependent. This dependence has been modelled phenomenologically using internal variables by a number of authors including Rice [13], Lagneborg [14], Miller [15, 16], Ponter and Leckie [17], and Robinson [18]. Robinson's model was motivated by the observations of Swindeman [19] in 304 stainless steel, who found that stress relaxation in the samples held at constant strain over a fixed time interval was strongly dependent on its prior deformation. In this model, creep and plasticity are accounted for simultaneously as irreversible inelastic deformation processes driven by a single thermodynamic force. The model includes a tensorial internal parameter, the backstress, whose evolution produces kinematic hardening for the viscoplastic yield surface. Robinson's model was extended by Murakami and Ohno [20], by the introduction of creep hardening surfaces. Peng and Zeng [21] proposed a generalised endochronic creep-plasticity theory without a yield surface.

Despite assuming the internal variable-free history-independent creep constitutive relationship, Eq. (1), a number of models of creep crack growth successfully capture the crack propagation observed experimentally. It is the objective of the present note to inquire into the reason for their predictive success. To this end, a cracked compact tension specimen obeying Robinson's constitutive law, henceforth referred to as the 'Robinson specimen', is considered. The material constants of an equivalent Norton's power-law material are deduced so as to match the steady state response of the Robinson material during uniaxial tensile tests. The 'Norton specimen' is identical to the Robinson specimen, except for the creep constitutive law, which is taken to be the history-independent equivalent Norton's power-law. For two types of damage evolution, viz., a stress-based law, and an inelastic strain-based law, the time to failure of material points ahead of the crack tip, in the crack plane, predicted in the two specimens are compared. It is found that in compact tension specimens subjected to dead loading, the influence of the constitutive model can be subsumed into the damage law. In other words, the time to failure predicted in the Norton specimen can be matched to that in the Robinson specimen simply by a change of the damage parameter in the former. This is true for both stress-based and inelastic strain-based damage laws.

Two significant simplifying restrictions imposed presently must be noted: (i) The crack is assumed to be stationary and (ii) the damage evolution law and constitutive laws are presently assumed to be uncoupled with each other, in contrast to e.g., Eq. (1). The former assumption corresponds to the limit whereat the time-scale associated with crack propagation is much larger than that of creep deformation, i.e., to slow crack growth. The former assumption will apply also during the crack initiation period [1, 22, 23]. Assumption (ii) enables damage evolution offline of the finite element simulations. Since the offline calculation corresponds to larger normal stresses ahead of the crack tip, the times to failure predicted following assumption (ii) will be conservative.

The constitutive laws and damage models studied are first reviewed in Sec. 2. Numerical experiments performed on compact tension specimen are then described, and their predictions compared in Sec. 3. The implications are then discussed in Sec. 4.

2. Constitutive laws and damage models

2.1. Robinson's constitutive law

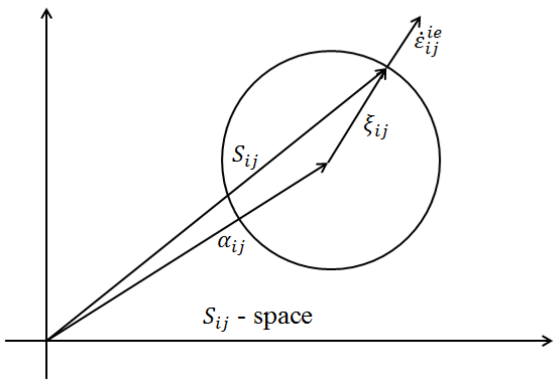

Figure 1: Geometric interpretation of Robinson's [18] creep constitutive law. S_{ij} denotes the imposed deviatoric stress, α_{ij} the kinematic back stress, and ξ_{ij} the effective stress. The circular yield locus demarcates the elastic zone from the inelastic one.

The constitutive law due to Robinson [18] represents deformation rate due to both creep and plasticity using the tensorial deviatoric strain-rate, $\dot{\varepsilon}_{ij}^{\mathrm{ie}}$. The strain-rate is taken to depend on the imposed deviatoric stress S_{ij} following:

$$2\mu_0\dot{\varepsilon}^{\mathrm{ie}}_{ij} = \begin{cases} F^{\frac{n-1}{2}}\xi_{ij}, & \text{if } F > 0, S_{ij}\alpha_{ij} > 0 \text{ and } S_{ij}\xi_{ij} > 0 \\ 0, & \text{if } F > 0, S_{ij}\alpha_{ij} > 0 \text{ and } S_{ij}\xi_{ij} \leq 0 \\ 0, & \text{if } F \leq 0. \end{cases} \tag{2}$$

In Eq. (2), α_{ij} represents the tensorial back stress, and ξ_{ij} represents the effective stress, defined as $\xi_{ij} = S_{ij} - \alpha_{ij}$. $F(\xi_{ij}) = \frac{1}{2}\xi_{ij}\xi_{ij}/k^2 - 1 = 0$ denotes the yield locus of radius k. The back stress evolves following:

$$\dot{\alpha}_{ij} = \begin{cases} \frac{2\mu_0 H}{G^{\beta/2}}\dot{\varepsilon}^{\mathrm{ie}}_{ij} - RG^{\frac{n-\beta-1}{2}}\alpha_{ij}, & \text{if } G > G_0 \text{ and } S_{ij}\alpha_{ij} > 0 \\ \frac{2\mu_0 H}{G_0^{\beta/2}}\dot{\varepsilon}^{\mathrm{ie}}_{ij} - RG_0^{\frac{n-\beta-1}{2}}\alpha_{ij}, & \text{if } G \leq G_0 \text{ and } S_{ij}\alpha_{ij} \leq 0, \end{cases} \tag{3}$$

where,

$$G = \alpha_{ij}\alpha_{ij}/(2k^2). \tag{4}$$

The circle in Fig. 1 represents the Robinson's yield surface centered at the current back stress α_{ij} with radius k. The applied stress S_{ij} imposed on the material point produces an effective stress ξ_{ij} due to the back stress. The inelastic strain rate is normal to the yield surface, following Eq. (2), so that the flow rule is clearly associative.

Eq. (3a) describes the evolution of the kinematic back stress α_{ij} in the direction of $\dot{\varepsilon}^{\mathrm{ie}}_{ij}$ and a simultaneous annihilation in the direction of the current value of the backstress, α_{ij}. These processes are controlled by rate constants H and R, respectively. Eq. (3a) becomes degenerate as $G \downarrow 0$; Eq. (3b) represents a regularisation of the first case in this limit purposed to avoid numerical degeneracies.

Under constant applied $\dot{\varepsilon}^{\mathrm{ie}}_{ij}$ or S_{ij}, the backstress, α_{ij} will evolve to a steady state and saturate. This helps the constitutive law capture both primary and secondary creeping response. According to Eqs. (2) and (3), an evolving α_{ij} characterises the former and a saturated α_{ij} the latter. Let $\alpha^{\mathrm{ss}}_{ij}$ denote the saturated value of the backstress under constant $\dot{\varepsilon}^{\mathrm{ie}}_{ij}$. Substituting $\dot{\alpha}_{ij} = 0$ in Eq. (3a), the steady-state or saturated backstress $\alpha^{\mathrm{ss}}_{ij}$ is given by

$$\alpha^{\mathrm{ss}}_{ij} = \frac{2\mu_0 H}{R\left[\frac{2[\mu_0 H]^2}{[Rk]^2}\right]^{\frac{n-1}{2n}}} \frac{\dot{\varepsilon}^{\mathrm{ie}}_{ij}}{(\dot{\varepsilon}^{\mathrm{ie}}_{kl}\dot{\varepsilon}^{\mathrm{ie}}_{kl})^{\frac{n-1}{2n}}}. \tag{5}$$

Use has been made of $G^{\mathrm{ss}} = \alpha^{\mathrm{ss}}_{ij}\alpha^{\mathrm{ss}}_{ij}/(2k^2)$ obtained from Eq. (4) in deriving Eq. (5). Eq. (5) implies that $\alpha^{\mathrm{ss}}_{ij}$ is parallel in stress space to $\dot{\varepsilon}^{\mathrm{ie}}_{ij}$, i.e., in Fig. 1, $\dot{\varepsilon}^{\mathrm{ie}}_{ij}$ points in the direction of the join of the origin and $\alpha^{\mathrm{ss}}_{ij}$.

An expression of $\alpha^{\mathrm{ss}}_{ij}$ in terms of stresses is obtained by substituting Eq. (2a) into Eq. (5). Let $A = 2\mu_0 H/R \left[2[\mu_0 H]^2/[Rk]^2\right]^{\frac{n-1}{2n}}$. Then,

$$
\begin{aligned}
\alpha_{ij}^{\mathrm{ss}} &= \frac{A}{[2\mu_0]^{1/n}} \frac{F^{\frac{n-1}{2n}}}{[(S_{kl}-\alpha_{kl}^{\mathrm{ss}})(S_{kl}-\alpha_{kl}^{\mathrm{ss}})]^{\frac{n-1}{2n}}}(S_{ij}-\alpha_{ij}^{\mathrm{ss}}), \\
&= \frac{A}{[2\mu_0]^{1/n}} \left[\frac{1}{2k^2} - \frac{1}{(S_{kl}-\alpha_{kl}^{\mathrm{ss}})(S_{kl}-\alpha_{kl}^{\mathrm{ss}})}\right]^{\frac{n-1}{2n}} (S_{ij}-\alpha_{ij}^{\mathrm{ss}}).
\end{aligned}
\tag{6}
$$

Eq. (6) indicates that the tensors $\alpha_{ij}^{\mathrm{ss}}$ and $S_{ij} - \alpha_{ij}^{\mathrm{ss}}$ are parallel, which is tantamount to asserting that $\alpha_{ij}^{\mathrm{ss}}$ and S_{ij} are parallel:

$$\alpha_{ij}^{\mathrm{ss}} = C S_{ij} \tag{7}$$

Substituting Eq. (7) into Eq. (6) yields the following non-linear equation for scalar C:

$$C = \frac{A}{[2\mu_0]^{1/n}} \left[\frac{1}{2k^2} - \frac{1}{(1-C)^2(S_{ij}S_{ij})}\right]^{\frac{n-1}{2n}} [1-C] \tag{8}$$

2.2. Norton's Power Law

Norton's power law [24] relates the inelastic strain rate to stress in the secondary creep regime as:

$$\dot{\varepsilon}_{ij}^{\mathrm{ie}} = (3/2)B\sigma_e^{n-1}S_{ij}, \tag{9}$$

where, $\sigma_e = (3S_{ij}S_{ij}/2)^{1/2}$. The constants B and n in Eq. (9) are identified from the Robinson's law, Eq. (2a) corresponding to the special case of uniaxial tensile loading at constant Cauchy stress σ along, say the x_1 direction. This approach mimics the standard experimental procedure for identifying secondary creep constants.

In uniaxial tension, $S_{11} = 2\sigma/3$, $S_{22} = S_{33} = -\sigma/3$, and $S_{12} = S_{13} = S_{23} = 0$. $S_{ij}S_{ij} = 2\sigma/3$, and Eq. (9) reduces to

$$\dot{\varepsilon}_{11}^{\mathrm{ie}} = B\sigma^n. \tag{10}$$

B and n are obtained by fitting the steady-state $\dot{\varepsilon}_{11}^{\mathrm{ie}} - \sigma$ response determined from Eq. (2), i.e., the response after α_{11} converges to $\alpha_{11}^{\mathrm{ss}}$ using the equation 7 and 8.

2.3. Short and long time limits

Instantaneously after load application, the stress state in the specimen is identical to that given by linear elasticity [1]. At this instant, the crack tip stress fields are completely characterised by the linear elastic stress intensity factor, K [25]. With time, creep deformation develops to relax the near crack tip stresses. At long times, the stress field approach a steady-state, given by the Hutchinson-Rice-Rosengren field.

$$\sigma_{ij} = \left(\frac{C^*}{I_n\ B\ r}\right)^{1/(n+1)} \tilde{\sigma}_{ij}(\theta). \tag{11}$$

Here, r denotes the distance from the crack tip, and I_n a parameter dependent only on n. The intensity of this field is characterised by the C^* parameter. Expressions for K and C^* for compact tension specimens based on their geometry and material properties are given by Tada et al. [25] and Shih et al. [26], respectively.

2.4. Stress-based damage model

A simple and widely used expression for damage evolution [2, 1] is presently adopted:

$$\frac{d\omega}{dt}(r,t) = \frac{D\sigma_{nn}^{\chi}(r,t)}{(1+\phi)(1-\omega)^{\phi}}. \tag{12}$$

σ_{nn} denotes the opening component of stress acting normal to the fracture plane. The damage variable ω, which is assigned the value 0 before loading, evolves toward value 1 under the applied stress. However, ω does not correspond to a physically measurable quantity. r denotes the distance from the stationary crack tip to the material point under consideration. Integrating Eq. (12) at a fixed r yields

$$\int_0^t \sigma_{22}^{\chi}(r,\tau)d\tau = \frac{1}{D}[(1-\omega_1)^{1+\phi} - (1-\omega_2)^{1+\phi}]. \tag{13}$$

Letting $\omega_1 = 0$ and $\omega_2 = 1$ and correspondingly letting $t = t_\mathrm{f}$, where t_f specifies the time to failure of the material point r ahead of the crack tip yields:

$$\int_0^{t_\mathrm{f}(r)} \sigma_{22}^{\chi}(r,\tau)d\tau = \frac{1}{D}. \tag{14}$$

For a given spatiotemporal variation of opening stress $\sigma_{nn}(r,t)$, Eq. (14) identifies $t_\mathrm{f}(r)$.

2.5. Inelastic strain-based damage model

Damage evolution based on Eq. (12) leads to mesh-dependence of the numerical results [27]. An alternative inelastic strain based damage evolution law, due to Nikbin et al. [3], states:

$$\frac{d\omega}{dt} = \frac{\dot{\varepsilon}_{nn}^{\mathrm{ie}}}{\varepsilon_\mathrm{f}}, \tag{15}$$

where ε_f denotes the limiting creep strain, or creep ductility of the material. ε_f also depends on the creep exponent and triaxiality. Again, ω evolves with deformation from 0 to 1; local failure is implied when $\omega = 1$. Integrating Eq. (15) in time, the local failure criterion is obtained as

$$\varepsilon_{nn}^{\mathrm{ie}}(t_\mathrm{f}) = \varepsilon_\mathrm{f}. \tag{16}$$

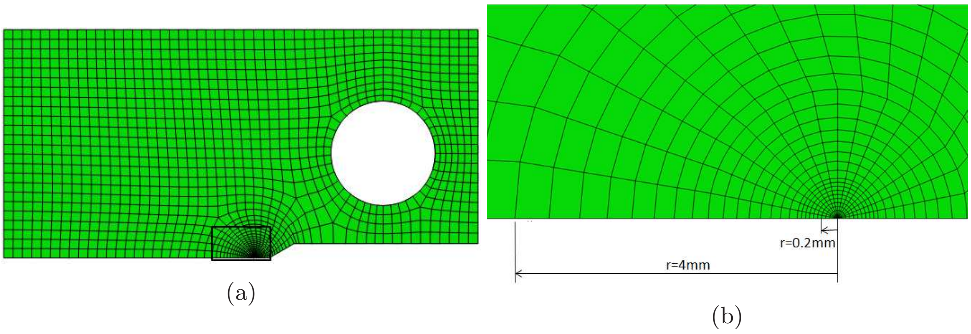

Figure 2: Finite element meshes of the (a) half compact tension specimen and (b) near crack-tip region.

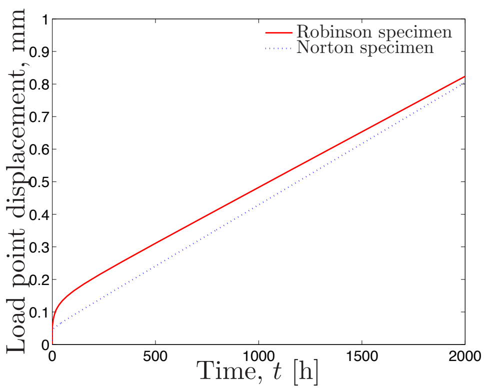

Figure 3: Load point displacement predicted for the Robinson and Norton specimen for the case of a stationary crack. The load point displacement evolves due to material deformation and not due to damage evolution or crack growth.

3. Results

Simulations are performed on a compact tension specimen, whose geometry matches that of compact tension specimen #10 in the experimental study of Maas and Pineau [22]. The ratio of the crack length to total length in this specimen is 0.34, and the specimen is crept at an applied load of 12070 N. Plane strain conditions are assumed. Large deformations are accounted for. The global and crack tip meshes are shown in Fig. 2. All the elements are quadratic brick elements with full integration.

The load point displacement predicted by both laws are shown in Fig. 3. The load point displacements obtained from the two models diverge most significantly from each other at short times, when the material is in undergoing primary creep according to Robinson's law, but secondary creep according to Norton's law. At longer times, the load point displacements converge by virtue of the convergence of the mechanical response predicted by both models. It is also important to note that both models do not account for damage evolution. Therefore, the load point displacements predicted in Fig. 3 are only a consequence of material deformation and not of material damage.

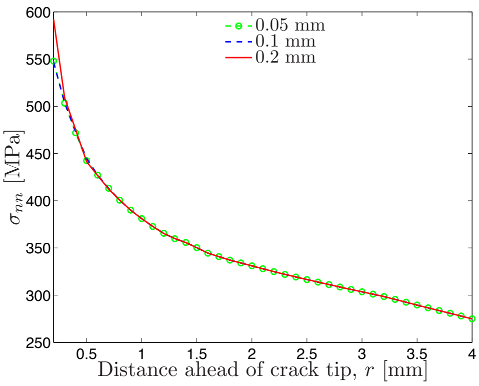

Figure 4: Sensitivity of the predicted normal stresses ahead of the crack tip to the mesh-size near the crack tip. Mesh sizes of 0.05 mm and 0.1 mm give practically identical predictions.

Robinson's constitutive law has been implemented as a user defined material (UMAT) in the finite element software, ABAQUS [28]. Details of the implicit time integration and consistent tangent modulus calculation are given in Appendix A. The crack-tip region is meshed finely. The mesh size near the crack tip is selected so as to eliminate mesh-sensitivity in the predicted stress fields. Fig. 4 shows the normal stress ahead of the crack tip predicted for three crack tip element sizes, 0.05 mm, 0.1 mm and 0.2 mm, 2000 h after load application, i.e., well after the establishment of a steady state creeping zone ahead of the crack tip. As seen, the stress variation predicted assuming the first two element sizes are practically identical. Therefore, the element size selected in all further calculations uses the smaller near-tip element size of 0.05 mm. Collapsed quarter-point quadratic elements surround the crack tip. The material parameters assumed correspond to 2¼ Cr-1 Mo steel at 600° C, given by Robinson [18]: $\mu_0 = 3 \times 10^7$ MPa h, $H = 0.001$/h, $R = 0.0001$/h, $k = 10$ MPa, $G_0 = 0.1$ MPa, and $n = 4$. Equivalent Norton law material parameters are determined as described in Sec. 2.2: $B = 3.467 \times 10^{-14}$ MPa^{-n}/h and $n = 4$. ABAQUS' in-built power-law constitutive law is used for simulations assuming Norton's law. Damage exponent $\chi = 6.2$ for 2¼ Cr-1 Mo steel [1]. For the present specimen, the mode I linear elastic stress intensity, as given by Tada et al. [25] works out to $K = 1189$ Nm$^{-3/2}$, and the steady state $C^* = 0.0532$ MPa mm/h according to Shih et al. [26]. Riedel and Rice [29], in considering the stress fields ahead of a crack tip, proposed a characteristic time t_1, given by

$$t_1 = K^2(1 - \nu^2)/[(n + 1)EC^*]. \tag{17}$$

They suggested that elastic fields prevail ahead of the crack tip up to time t_1 and termed this regime as brittle. For time $t > t_1$, they proposed assuming the time independent C^* field ahead of the crack tip, and termed this regime ductile. For the presently studied material, $t_1 \approx 0.03$ h. For the time durations considered, the present test conditions fall well within the ductile regime.

3.1. Stress fields

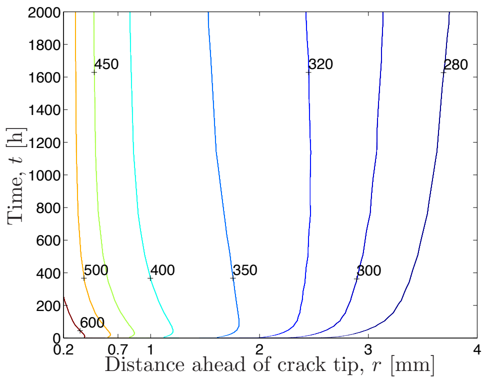

(a) Robinson specimen

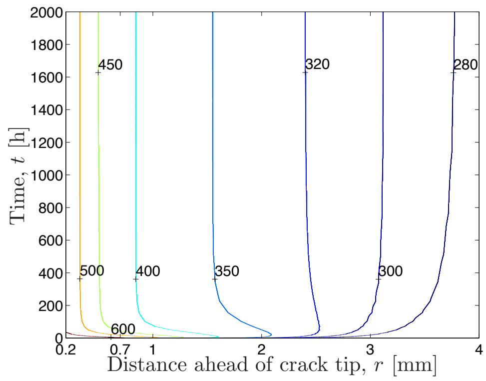

(b) Norton specimen

Figure 5: Predicted spatiotemporal variation of stress σ_{nn} in the crack plane, in the (a) Robinson and (b) Norton specimen.

Comparing the stress contours obtained from a finite element simulation assuming a linear elastic material with the asymptotic K field given by Tada et al. [25] (not shown) suggests that the region of K-dominance is limited to 0 mm $\leq r \leq$ 2 mm. A similar comparison of the steady-state asymptotic solution given by Shih et al. [26] with the long time finite element solution indicates that the C^*-dominated field also approximately has the same range.

The spatiotemporal variation of the opening stress component σ_{nn} predicted in the Robinson and Norton specimens is presented in Figs. 5a and 5b, respectively. In each of these figures, σ_{nn} coincides at $t = 0$ h with the linear elastic solution within the range of K-dominance and approaches the steady-state solution at $t = 2000$ h. The stress fields vary rapidly in both cases near $t = 0$ h. The rate of approach to the steady-state C^* field is faster in the Norton specimen, Fig. 5b, than in the Robinson specimen, Fig. 5a. The stress evolution with time predicted by both laws at each material point is seen to be non-monotonic over a certain range of r. The timescales considered here (hours) is orders of magnitude more than t_1, given by Eq. (17), for the present specimen. Yet, the stress-fields deviate substantially from the time-independent C^*-field given by Eq. (11).

The stress-states predicted by the time-independent C^* field (not shown) will plot as a series of straight vertical contours when depicted in the format of Fig. 5. It is clear that the stress-state in the Robinson and Norton specimen approach the C^* stress distribution only at very long times.

3.2. Primary and secondary creep

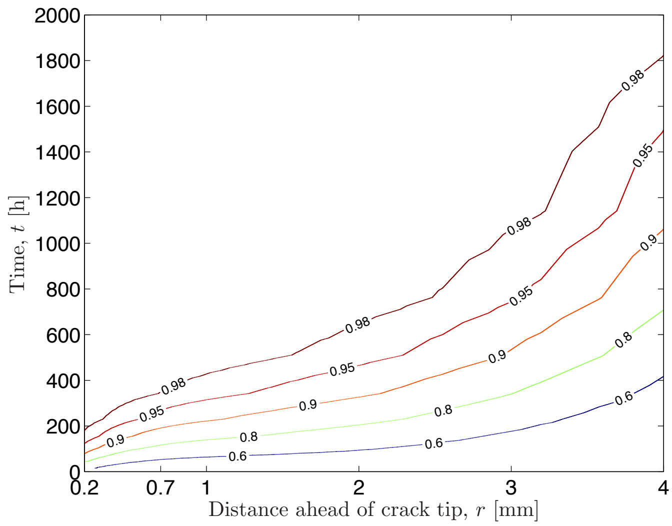

Figure 6: Spatiotemporal variation of $\alpha_{nn}/\alpha_{nn}^{\mathrm{ss}}$. $\alpha_{nn}/\alpha_{nn}^{\mathrm{ss}} \approx 1$ indicates secondary creep.

The stress fields in the Robinson and Norton materials differ because while Robinson's law accounts for primary creep through an evolving internal back-stress, α_{nn}, Norton's law does not. The ratio of the current back stress to the saturation back stress, $\alpha_{nn}(r,t)/\alpha_{nn}^{\mathrm{ss}}(r,t)$ at each spatiotemporal point indicates the stage of creep. $\alpha_{nn}(r,t)/\alpha_{nn}^{\mathrm{ss}}(r,t) \approx 1$ indicates secondary creep, while $\alpha_{nn}(r,t)/\alpha_{nn}^{\mathrm{ss}}(r,t) \ll 1$ indicates primary creep. Fig. 6 plots the spatiotemporal variation of $\alpha_{nn}(r,t)/\alpha_{nn}^{\text{ss}}(r,t)$ in the Robinson specimen. Secondary creep is first established close to the crack tip.

3.3. Time to failure

The times to failure, t_{f} given by Eqs. (14) and (16) predicted for the Robinson and Norton specimens using the two damage models of Sec. 2.4 and 2.5 are now compared. These times to failure are also compared against the time to failure predicted assuming the C^* field.

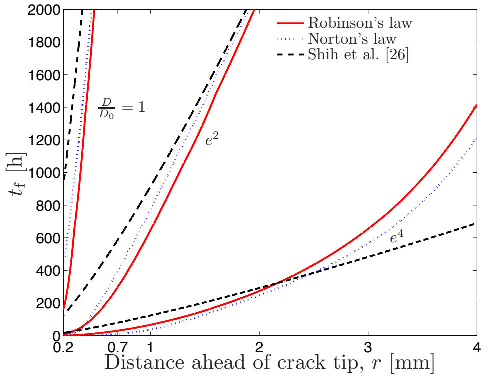

(a) Equal damage parameters.

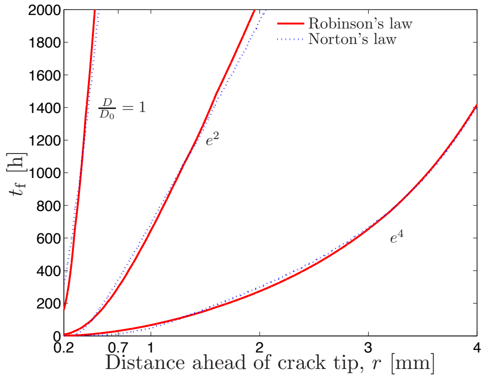

(b) Adjusted damage parameters.

Figure 7: Spatiotemporal variation of time to failure t_{f} ahead of a stationary crack, following the stress-based damage model (Sec. 2.4), (a) assuming the same parameter D associated with both constitutive laws, and (b) assuming different 'fitting' parameters associated with Norton's law, as given in Tab. 1.

Consider a reference damage rate coefficient $D_0 = 1.425 \times 10^{-21}$ MPa$^{-\chi}$ /h. Fig. 7a plots the spatial distribution of t_{f} for three assumed damage coefficients: $D/D_0 = 1$, e^2, and e^4. t_{f} decreases with increasing D, in accord with Eqs. (12), and (14). For small $D/D_0 = 1$ the rate of damage is slow and failure occurs at long times. The significantly damaged region, i.e., the process zone, is confined in this case near the crack tip. The rate of damage accumulation and the extent of the process zone increases with increasing D/D_0. It is reiterated that the time to failure, t_{f} is obtained presently under the assumption of a stationary crack. The reciprocal of the slope of the contour lines of constant D/D_0 shown in Fig. 7a should not be interpreted as the speed of crack propagation.

For small $D/D_0 = 1$, a smaller t_{f} is predicted in the Robinson specimen than in the Norton specimen. At larger $D/D_0 \geq e^2$, a switchover occurs: near the crack-tip, the Norton specimen has a smaller t_{f}, while away from the crack-tip, the Robinson specimen has a smaller t_{f}. The C^* field, being a lower bound on the stresses predicted by both Norton and Robinson laws, always over-predicts t_{f} relative to both.

Even though t_{f} predicted in the two specimen differ systematically, the possibility of 'fitting' the t_{f} predicted in the Robinson specimen by adjusting D

Table 1: Damage parameter D/D_0 used with Norton's law to 'fit' the time to failure, t_f, predictions obtained from Robinson's law.

D/D_0, Robinson's law	D/D_0, Norton's law
e^0	$e^{0.2}$
e^2	$e^{2.1}$
e^4	$e^{3.83}$

in the Norton specimen is now considered. Tab. 1 shows the adjusted D used in obtaining the fit shown in Fig. 7b. The largest deviations between the t_f predictions of the two models occur at the smallest $D/D_0 = 1$, and the smallest deviations at the largest $D/D_0 = e^4$.

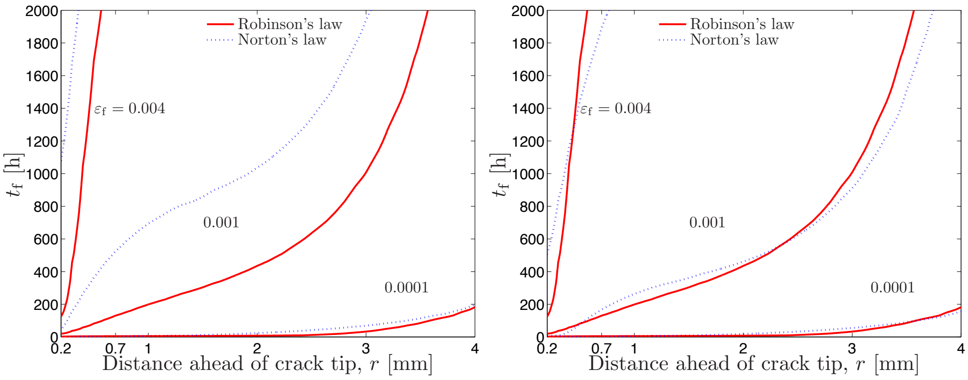

(a) Equal damage parameters.

(b) Adjusted damage parameters.

Figure 8: Spatiotemporal variation of time to failure t_f ahead of a stationary crack, following the inelastic strain-based damage model (Sec. 2.5), (a) assuming the same parameter ε_f associated with both constitutive laws, and (b) assuming different 'fitting' parameters associated with Norton's law, as given in Tab. 2.

Analogously, t_f predicted in the Robinson and Norton specimens using the inelastic strain-criterion, Eq. (16), are shown in Fig. 8a. t_f predicted in the two specimens are even more widely separated than in the stress-based model, for $\varepsilon_\mathrm{f} = 0.001$ and 0.004. It was attempted to match the t_f predicted in the Robinson specimen and with that obtained in the Norton specimen. The damage parameter ε_f in the latter specimen were modified in order to obtain the best match. The best match is shown in Fig. 8b. The corresponding ε_f used in conjunction with Norton's law are listed in Tab. 2. While reasonably good matches are obtained for all three ε_f considered, the quality of fit clearly improves with decreasing ε_f.

The times to failure, t_f, of material points ahead of a stationary crack were determined above for various D and $1/\varepsilon_\mathrm{f}$, in Figs. 7 and 8. Failure of material

Table 2: Damage parameter ε_f used in the Norton specimen to fit the time to failure, t_f, predictions obtained from the Robinson specimen.

ε_f, Robinsons's law	ε_f, Norton's law
0.004	0.00235
0.001	0.00062
0.0001	0.00008

points ahead of the crack tip corresponds to crack propagation. The mechanical fields ahead of a propagating crack will depend on the history of crack growth. For slow crack propagation, which corresponds to small D or $1/\varepsilon_\mathrm{f}$, the mechanical fields ahead of the propagating crack may still be approximated by those ahead of the presently considered stationary crack. For fast crack propagation corresponding to larger D or $1/\varepsilon_\mathrm{f}$, the stationary crack's mechanical fields will not apply even approximately [29]. The results presented in this section are therefore, physically meaningful only for small D or $1/\varepsilon_\mathrm{f}$.

4. Discussion and conclusions

It has been shown that the time to failure of material points ahead of a stationary crack predicted in a history-dependent Robinson specimen can be matched to those predicted in an equivalent history-independent Norton specimen simply by altering the damage parameter D or $1/\varepsilon_\mathrm{f}$ in the latter.

The present assumption of a stationary crack remains valid until the initiation time of crack propagation. This time, defined by Maas and Pineau [22] as the time needed for the crack to extend a microstructural distance of 50 μm, has been reported as 207 h, which is about one-sixth of the total test duration, for the presently studied specimen. When applied to this setting, the aforementioned result implies that the crack speed at the end of the initiation time in the Robinson specimen can be captured by a Norton specimen simply by a change of the damage parameter. If Robinson's law is taken to accurately describe the creep law of the physical material, this means that equal predictive accuracy is possible with the simpler history-independent Norton's law.

The present stationary crack may also be regarded as the limiting case of slow creep crack propagation, wherein the time scale of crack propagation is much larger than the time scale for the establishment of steady-state creep ahead of the crack tip [29, 30]. Consider the limit, opposite to that of the present study, of fast crack growth. In this limiting case, the time scale associated with crack growth will be much smaller than that associated with creep deformation. Crack growth will occur in a predominantly linear elastic specimen, with creep strains being appreciable only near the crack tip [29]. In this case, the specific creep constitutive model will cease to be important. Therefore, no adjustment will be needed in the damage parameter D or $1/\varepsilon_\mathrm{f}$ to match predictions obtained from the Robinson and Norton specimens.

Next, consider the case of a crack propagating at any non-zero speed. In this case, the mechanical fields ahead of the crack tip will depend on the prior history of crack growth. It is interesting to ask if the present result will also apply to this case. That is, can the damage evolution predicted ahead of a propagating crack in a Robinson material also be captured by Norton's law by adjusting the damage parameters? While the present work does not directly address this question, the foregoing considerations suggest an affirmative answer in both limiting cases of slow and fast crack growth. This suggests that it may be possible to obtain equivalent damage parameters for any intermediate crack speed. However, the adjusted damage parameters may vary with crack speed. If this variation were significant, the damage parameters used in the aforementioned works may need modification in order to be applicable to other loading conditions producing markedly different crack speeds.

In the single loading condition studied, Oh et al. [10] and Wen et al. [11], obtained excellent agreement between experiment and model predictions using history-independent constitutive laws. This further suggests the existence of a valid damage parameter adjustment corresponding to their loading condition. However, if the variation in the adjusted damage parameters with crack speed were significant, the damage parameters used in the aforementioned works may need modification in order to be applicable to other loading conditions producing markedly different crack speeds.

As noted in Sec. 3.3, for the stationary crack, which is the limiting case of slow crack growth, only small values of the damage parameters D or $1/\varepsilon_{\mathrm{f}}$ are physically meaningful. This regime corresponds to significant damage accumulation only near the crack-tip. In the case of fast crack propagation too, the zone of significant damage, i.e., the process zone, will be confined well within the 'small scale yielding zone', defined by Riedel and Rice [29]. The smallness of the process zone in both limiting cases suggests that the same will be true for any crack propagation speed. This implies that the load point displacement must only be slightly affected by the damage evolution; the bulk of its contribution must arise from crack opening and material creep deformation. During the initiation period for creep crack growth, the latter contribution will dominate, and as shown in Fig. 3, will be sensitive to the creep constitutive law. The accuracy of the assumed creep constitutive law can be judged by comparing the predicted and measured load point displacements at small times. At long times, creep deformation of both Robinson and Norton specimens approach each other, and in any case, the dominant contribution to the load point displacement is from the crack opening. Therefore, load point displacements will not be sensitive to the creep constitutive law at long times.

[1] H. Riedel, Fracture at high temperatures, Materials research and engineering, Springer-Verlag, Berlin, 1987.

[2] D. Hayhurst, P. Brown, C. Morrison, The role of continuum damage in creep crack growth, Philosophical Transactions of the Royal Society of London. Series A, Mathematical and Physical Sciences 311 (1516) (1984) 131–158.

[3] K. Nikbin, D. Smith, G. Webster, Prediction of creep crack growth from uniaxial creep data, Proc. R. Soc. Lond. A. 396 (1810) (1984) 183–197.

[4] K. Saanouni, J. L. Chaboche, C. Bathias, On the creep crack growth prediction by a local approach, Eng. Fract. Mech. 25 (5) (1986) 677–691.

[5] M. Yatomi, K. Nikbin, N. O'Dowd, Creep crack growth prediction using a damage based approach, Int. J. Pres. Ves. Pip. 80 (7) (2003) 573–583.

[6] M. Yatomi, N. ODowd, K. Nikbin, G. Webster, Theoretical and numerical modelling of creep crack growth in a carbon–manganese steel, Eng. Fract. Mech. 73 (9) (2006) 1158–1175.

[7] D. Dean, D. Gladwin, Creep crack growth behaviour of Type 316H steels and proposed modifications to standard testing and analysis methods, International Journal of Pressure Vessels and Piping 84 (6) (2007) 378–395.

[8] M. Yatomi, C. M. Davies, K. M. Nikbin, Creep crack growth simulations in 316H stainless steel, Eng. Fract. Mech. 75 (18) (2008) 5140–5150.

[9] T. Hyde, M. Saber, W. Sun, Testing and modelling of creep crack growth in compact tension specimens from a {P91} weld at 650°C, Eng. Fract. Mech. 77 (15) (2010) 2946–2957.

[10] C.-S. Oh, N.-H. Kim, Y.-J. Kim, C. Davies, K. Nikbin, D. Dean, Creep failure simulations of 316H at 550°C: Part I A method and validation, Eng. Fracture Mech. 78 (17) (2011) 2966–2977.

[11] J.-F. Wen, S.-T. Tu, X.-L. Gao, J. Reddy, Simulations of creep crack growth in 316 stainless steel using a novel creep-damage model, Eng. Fracture Mech. 98 (2013) 169 – 184.

[12] J.-F. Wen, S.-T. Tu, X.-L. Gao, J. N. Reddy, New model for creep damage analysis and its application to creep crack growth simulations, Mater. Sci. Tech. 30 (1) (2014) 32–37.

[13] J. R. Rice, On the structure of stress-strain relations for time-dependent deformation of metals, J. Appl. Mech. (1970) 728.

[14] R. Lagneborg, A Modified Recovery-Creep Model and Its Evaluation, Metal Sci. 6 (1) (1972) 127–133.

[15] A. A. Miller, An Inelastic Constitutive Model for Monotonic, Cyclic, and Creep Deformation: Equations Development and Analytical Procedures, ASME. J. Eng. Mater. Technol. 98 (2) (1976) 106–112.

[16] A. A. Miller, An Inelastic Constitutive Model for Monotonic, Cyclic, and Creep Deformation: Application to Type 304 Stainless Steel, ASME. J. Eng. Mater. Technol. 98 (2) (1976) 97–105.

[17] A. R. S. Ponter, F. A. Leckie, Constitutive Relationships for ., the Time-Dependent Deformation of Metals, ASME. J. Eng. Mater. Technol. 98 (1) (1976) 47–51.

[18] D. N. Robinson, A Unified Creep-Plasticity Model for Structural Metals at High Temperature, Tech. Rep. ORNL/TM-5969, Oak Ridge National Laboratory, 1978.

[19] R. W. Swindeman, Isochronous Relaxation Curives for Type 304 Stainless Steel After Monotonic and Cyalic Strain, Tech. Rep. ORNL/TM-6380, Oak Ridge National Laboratory, 1978.

[20] S. Murakami, N. Ohno, A constitutive equation of creep based on the concept of a creep-hardening surface, Int. J. Solids Struct. 18 (7) (1982) 597–609.

[21] X. Peng, X. Zeng, J. Fan, A physically based description for coupled plasticity and creep deformation, Int. J. Solids Struct 35 (21) (1998) 2733–2747.

[22] E. Maas, A. Pineau, Creep crack growth behavior of type 316L steel, Eng. Fract. Mech. 22 (2) (1985) 307–325.

[23] P. Bensussan, E. Maas, R. Pelloux, A. Pineau, Creep crack initiation and propagation: fracture mechanics and local approach, J. Pressure Vessel Tech. 110 (1) (1988) 42–50.

[24] F. H. Norton, Creep of steel at high temperatures, McGraw Hill, 1929.

[25] H. Tada, P. C. Paris, G. R. Irwin, The Stress Analysis of Cracks Handbook. The American Society of Mechanical Engineers, New York .

[26] C. Shih, V. Kumar, M. German, An engineering approach for elastic-plastic fracture analysis, EPRI NP-1931, RP1237-1 (July 1981) .

[27] S. Murakami, Y. Liu, M. Mizuno, Computational methods for creep fracture analysis by damage mechanics, Comput. Method. Appl. M. 183 (1) (2000) 15–33.

[28] Hibbitt, Karlsson, Sorensen, ABAQUS/Standard: User's Manual, no. ver. 6.10 in ABAQUS/Standard: User's Manual, Hibbitt, Karlsson & Sorensen, 2010.

[29] H. Riedel, J. R. Rice, Tensile cracks in creeping solids, in: Fracture Mechanics: 12th Conference, ASTM International, 112, 1980.

[30] H. Riedel, Creep deformation at crack tips in elastic-viscoplastic solids, J. Mech. Phys. Solids 29 (1) (1981) 35–49.

[31] J. C. Simó, T. J. Hughes, Computational Inelasticity, Springer-Verlag, Berlin, 1998.

[32] J. Ronda, G. J. Oliver, Comparison of applicability of various thermo-viscoplastic constitutive models in modelling of welding, Comput. Methods Appl. Mech. Engrg. 153 (1998) 195–221.

Appendix A. Numerical implementation of Robinson's law

Appendix A.1. Implicit time integration

Numerical integration must be used to solve the ordinary differential equations in the constitutive model. The backward Euler method is used for numerical integration due to its unconditional stability [31]. The generalized backward (implicit) Euler equation for the evolution of an arbitrary variable X between time steps m and $m+1$ follows:

$$X_{m+1} = X_m + \Delta t \dot{X}_{m+1} \tag{A.1}$$

The inelastic strain rate in Robinson's model, Eq. (2), may be expressed as:

$$\dot{\boldsymbol{\varepsilon}}^{\mathrm{ie}} = \gamma \hat{\boldsymbol{n}} \tag{A.2}$$

where, $\gamma = \left[F^{\frac{n-1}{2}}/2\mu_0\right] \|\xi_{ij}\|$ represents the equivalent plastic strain rate, and $\hat{\boldsymbol{n}} = \boldsymbol{\xi}/\|\boldsymbol{\xi}\|$ is the normal to the yield surface. Applying the backward Euler method, Eq. (A.1), to Eq. (A.2) yields:

$$\boldsymbol{\varepsilon}^{\mathrm{ie}}_{m+1} = \boldsymbol{\varepsilon}^{\mathrm{ie}}_{m} + \Delta\gamma_{m+1} \hat{\boldsymbol{n}}_{m+1} \tag{A.3}$$

where,

$$\Delta\gamma_{m+1} = \gamma_{m+1}\Delta t = \left[\frac{F_{m+1}^{\frac{n-1}{2}}}{2\mu_0}\right] \|\boldsymbol{\xi}_{m+1}\| \Delta t. \tag{A.4}$$

Similarly, one can also apply backward Euler method for the internal stress evolution, given by Eq. (3):

$$\boldsymbol{\alpha}_{m+1} = \boldsymbol{\alpha}_m + \left[\frac{2\mu_0 H}{G^{\beta/2}} \dot{\boldsymbol{\varepsilon}}^{\mathrm{ie}} - R G^{\frac{n-\beta-1}{2}} \boldsymbol{\alpha}\right]_{m+1} \Delta t. \tag{A.5}$$

This can be simplified as

$$\boldsymbol{\alpha}_{m+1} = \boldsymbol{\alpha}_m + K_1 \hat{\boldsymbol{n}}_{m+1} - K_2 \boldsymbol{\alpha}_{m+1}, \tag{A.6}$$

where,

$$K_1 = \frac{2\mu_0 H \Delta\gamma_{m+1}}{\left[\frac{\alpha_{m+1}:\alpha_{m+1}}{2k^2}\right]^{\beta/2}}, \quad \text{and} \quad K_2 = R\Delta t \left[\frac{\boldsymbol{\alpha}_{m+1} : \boldsymbol{\alpha}_{m+1}}{2k^2}\right]^{\frac{n-\beta-1}{2}}.$$

The classical radial return mapping algorithm [31] is used to estimate unknown stress tensor and the internal stress tensor at time step $m+1$. Following this method, a trial stress tensor $\|\boldsymbol{\xi}^{\mathrm{trial}}_{m+1}\|$ is estimated assuming that the strain increment is purely elastic. The trial stress and radial return are depicted in Fig. (A.9). Following the standard procedure, the effective stress tensor at time $m+1$ is obtained as

$$\|\boldsymbol{\xi}_{m+1}\| = \|\boldsymbol{\xi}^{\mathrm{trial}}_{m+1}\| - [K_3 + 2\mu]\Delta\gamma_{m+1} + K_2 \boldsymbol{\alpha}_{m+1} : \hat{\boldsymbol{n}}_{m+1}. \tag{A.7}$$

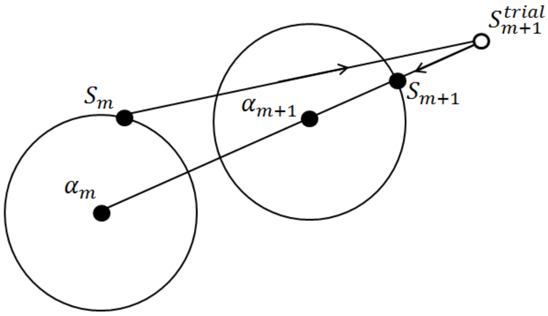

Figure A.9: Geometric interpretation of the return mapping algorithm with kinematic hardening [31]

Appendix A.2. Consistent tangent modulus

In computing the material response, ABAQUS imposes a strain-increment at each element integration point [31]. The user-material, or UMAT subroutine fed into ABAQUS must update the stress tensor, internal variables and also the tangent modulus to the end of the imposed strain increment. The tangent modulus is the rate of change of incremental Cauchy stress tensor $\boldsymbol{\sigma}$ with respect to the incremental strain tensor $\boldsymbol{\varepsilon}$.

The consistent tangent modulus [31, 32] accounts for the algorithmic procedure of determining the stress-state at the end of the imposed strain increment, in contrast to the elastoplastic tangent modulus which does not account for the radial return algorithm and depends only on the constitutive law.

Assuming a Hookean elastic material, the expression for stress tensor at the end of the strain-increment $m+1$ can written as:

$$\boldsymbol{\sigma}_{m+1} = \kappa(\text{trace}[\boldsymbol{\varepsilon}_{m+1}]) + 2\mu(\boldsymbol{e}_{m+1} - \Delta\gamma\hat{\boldsymbol{n}}_{m+1}), \tag{A.8}$$

where $\boldsymbol{e}$ is the deviatoric strain, and where κ and μ denote the bulk and shear moduli, respectively. Differentiating Eq. (A.8) with respect to strain tensor $\boldsymbol{\varepsilon}_{m+1}$ and by using the chain rule,

$$\frac{d\boldsymbol{\sigma}_{m+1}}{d\boldsymbol{\varepsilon}_{m+1}} = \kappa\mathbf{1}\otimes\mathbf{1} + 2\mu[\boldsymbol{I} - \frac{1}{3}\mathbf{1}\otimes\mathbf{1}] - 2\mu\hat{n}_{m+1}\otimes\frac{\partial\Delta\gamma_{m+1}}{\partial\varepsilon_{m+1}} - 2\mu\Delta\gamma\frac{\partial\hat{n}_{m+1}}{\partial\boldsymbol{\varepsilon}_{m+1}} \tag{A.9}$$

is obtained. Here, $\mathbf{1}$ and $\boldsymbol{I}$ denote identity tensors of rank 2 and 4, respectively.

Substituting Eq. (A.4) and Eq. (A.5) into Eq. (A.9, and performing algebraic manipulations yields the final form of consistent tangent modulus tensor as

$$\frac{\partial\boldsymbol{\sigma}_{m+1}}{\partial\boldsymbol{\varepsilon}_{m+1}} = \left[\frac{3\kappa - 2\mu D_1}{3}\right]\mathbf{1}\otimes\mathbf{1} + 2\mu D_1\boldsymbol{I} - 2\mu D_2\hat{\boldsymbol{n}}_{m+1}\otimes\hat{\boldsymbol{n}}_{m+1} \tag{A.10}$$

where,

$$D_1 = 1 - \frac{2\mu\Delta\gamma_{m+1}}{\|\boldsymbol{\xi}_{m+1}^{\text{trial}}\|},$$

$$D_2 = \left[C_2 - \frac{2\mu\Delta\gamma_{m+1}}{\|\boldsymbol{\xi}_{m+1}^{\text{trial}}\|} \right],$$

$$C_1 = \frac{\partial\Delta\gamma_{m+1}}{\partial\|\boldsymbol{\xi}_{m+1}\|}, \qquad \text{and}$$

$$C_2 = \frac{2\mu C_1}{1 - K_4 C_1}.$$